Structures and Antifouling Properties of Self-assembled Zwitterionic Peptide Monolayers: Effects of Peptide Charge Distributions and Divalent Cations

Chuanxi Li [†, ‡, §, #], Chunjiang Liu [†, #], Minglun Li [‡], Xin Xu [‡], Shuzhou Li [‡*], Wei Qi [†, §], Rongxin Su [†, §, *], Jing Yu [‡, *]

[†] State Key Laboratory of Chemical Engineering, Tianjin Key Laboratory of Membrane Science and Desalination Technology, School of Chemical Engineering and Technology, Tianjin University, Tianjin 300072, PR China

[‡] School of Materials Science and Engineering, Nanyang Technological University, Singapore 639798, Singapore

[§] Collaborative Innovation Center of Chemical Science and Engineering (Tianjin), Tianjin 300072, PR China

KEYWORDS: zwitterionic, peptide, antifouling, charge distribution, divalent cations

ABSTRACT

Zwitterionic peptides are great candidates as antifouling coating materials in many biomedical applications. We investigated the structure and antifouling properties of surface tethered zwitterionic peptide monolayers with different peptide chain lengths and charge distributions using a combination of surface plasma resonance (SPR), atomic force microscopy (AFM), and all atomistic molecular dynamics (MD) simulation techniques. Our results demonstrate that longer zwitterionic peptides exhibit better antifouling performance. The patchy charge distributions of the positive and negative charges in the peptides, although affecting the structure of the peptide molecules, do not significantly change the antifouling properties of the peptide monolayers in solution containing monovalent. However, divalent cations, Ca^{2+} and Mg^{2+}, in solution can significantly alter the structure and lower the antifouling performance of the zwitterionic peptide monolayers, especially with the sequences of patchy charge distributions. All atomistic MD simulations quantitatively reveal that the divalent cations in solution lead to more inter-chain electrostatic crosslinks between peptide chains, especially for peptides with patchy charges, which causes dehydration of the zwitterionic peptides and diminishes their antifouling performances.

INTRODUCTION

Biofouling is a serious challenge in a wide range of systems, such as medical implants[1], drug delivery carriers[1-4], biosensors[5, 6], and water purification systems[7, 8]. More than 45% of hospital-contracted infections are traced to biofilm-infected medical devices and estimates show that 10% of hospital patients will contract an infection from a clinical implant.[9] Despite of the considerable efforts spent over the past decades on preventing the nonspecific adsorption

of biomacromolecules, bacterial and microorganisms, an effective antibiofouling strategy on various surfaces is still lacking.[10, 11] Surface tethered polymers, especially polyethylene glycol (PEG) related materials have long been proposed as effective antifouling materials due to their strong hydration[12, 13], which effectively prevents the adsorption of fouling molecules.[14-18] But PEG is susceptible to oxidative degradation in the presence of air, and its immunogenicity also significantly limits its application in many biomedical applications. [19-22] Developing next generation antibiofouling coating materials is of great importance to many practical applications.[7, 23, 24]

Recently, zwitterionic polymers received great attention due to their better performance to substitute PEG.[10, 25-27] Carrying equal positive and negative charges in the same functional motif, zwitterionic polymers such as poly(2-methacryloyloxyethyl phosphorylcholine) (PMPC), poly(sulfobetaine methacrylate) (PSBMA), and poly(carboxybetaine methacrylate) (PCBMA) have strong hydration while maintaining overall charge neutrality in aqueous solutions, and therefore show superior antifouling performance than many other polymers.[27-36]

Zwitterionic peptides are peptides consisting of alternating positively charged and negatively charged amino acid residues.[37] Comparing to the zwitterionic polymers, the compositions, structure, and chain length of the zwitterionic peptides can be very well tuned through controlling the peptide sequences in solid state peptide synthesis.[38, 39] There are a variety of natural and synthetic amino acids can be utilized to tune the properties of the peptides. It has been shown that adding a PPPP motif can increase the packing density of the self-assembled peptide monolayers and improve the antifouling properties of the surface grafted zwitterionic peptide.[40] Such advantages have been exploited for engineering various

zwitterionic peptides for various applications, such as surface functionalization of implants[41], biosensors[42, 43] , drug delivery[44, 45], and antifouling applications.[46-48]

Various parameters, including the peptides sequences, chain length, charge distribution, and solution ionic environment can affect the antifouling properties of the surface tethered zwitterionic peptide.[49, 50] Chen *et al.* investigated the effect of monovalent ions to the antifouling properties of lysine-glutamic acid mixed charge polypeptide thin films.[49] Higher lysozyme adsorption was observed under relatively low ionic strength conditions. Ziemba *et al.* designed a block copolymer (BCP) of polystyrene and a zwitterionic peptide comprising repeated units of lysine-glutamic acid, and concluded that the grafting density of the peptides is critical for the antifouling performance of the zwitterionic peptides.[51] Despite of numerous efforts in developing antifouling zwitterionic antifouling polymeric and peptidyl materials, many fundamental questions that are critical to the application of zwitterionic materials still remain to be answered. In commonly studied zwitterionic peptides, the positive and negative charges are arranged alternatively. Yet it is not fully clear whether having patchy charges in the peptides, e.g. having multiple positive charges next to the same amount of negative charges, would affect the structural and properties of the zwitterionic peptides.[50] Another important question that is critical to the antifouling application of zwitterionic peptides is the effect of multivalent ions in the solution environment.[52] The existence of multivalent ions can dramatically affect the structure and properties of polyelectrolyte in solution.[53-55] However, their effects on many zwitterionic polymers and peptides are still not fully understood.[51] Considering the wide existence of multivalent ions in natural and biological environment, gaining a better understanding on the effect of multivalent ions to the antifouling properties of

the zwitterionic materials is critical.

In this work, we took the advantage of well-defined structure of zwitterionic peptides and tested a series of zwitterionic peptides with well controlled chain length and different patchy charge distributions. We systematically investigated their antifouling properties in the presence of Ca^{2+} and Mg^{2+} ions using a combination of surface plasma resonance (SPR), atomic force microscopy (AFM) and all atomistic molecular dynamics (MD) simulation techniques. Our results demonstrate that the chain length and the charge distributions of the zwitterionic peptides can affect the antifouling performance of the peptides, especially in solutions containing divalent cations.

RESULTS AND DISCUSSION

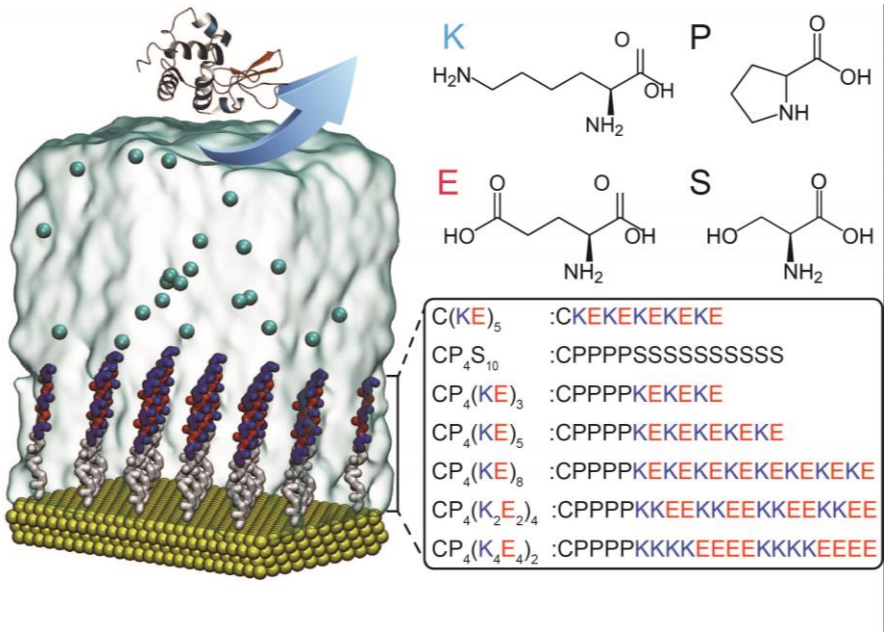

Scheme 1. A schematic of the zwitterionic peptide modified gold surface and the sequences of the peptides studied.

We systematically designed 5 zwitterionic peptides containing alternating positively charged lysine (K) and negatively charged glutamine (E) residues. Three peptides, $CP_4(KE)_3$, $CP_4(KE)_5$, and $CP_4(KE)_8$, are synthesized to test the effect of increasing KE repeating unit. The 4 prolines (PPPP) were included to facilitate the assembly of the peptides. A cysteine is used as the end anchoring group on gold surfaces via the well-established thiol-gold chemistry. A peptide with the sequence of $C(KE)_5$ was used as a control sample to confirm the effect of the PPPP unit. Another series of peptides with the same number of amino acid residues but different charge distributions, $CP_4(KE)_8$, $CP_4(K_2E_2)_4$, and $CP_4(K_4E_4)_2$, were used to investigate the effect of patchy charge distributions.

The effect of charge distribution

We first investigated the assembly behavior of the zwitterionic peptides on gold surface. After the peptide modification, the contact angle of the gold surface decreased from 81.5° to 17.2°-28.6° (Figure 1a), suggesting the successful modification of the gold surfaces by the zwitterionic peptides. We then investigated the antifouling performance of the zwitterionic peptides using the SPR technique (Figure 1b). Each zwitterionic peptide was first grafted onto a gold substrate by flowing 0.015 mM peptide solution through the SPR chamber with a flow rate of 5 μL/min for 40 min. The growth of the peptide monolayer was monitored in real time. The final grafting density of the peptides decreases as the chain length of the peptide increases. As the number of amino acid increased from 11 to 21, the grafting density decreased from 0.10 nmol/cm^2 to 0.06 nmol/cm^2, correspond to 0.60 chain/nm^2 to 0.37 chain/nm^2 respectively (Figure 1c). For peptides with the same chain length, $CP_4(KE)_3$ and $C(KE)_5$, having the PPPP unit can significantly increase the grafting density of the peptides due to the covalently

constrained backbone of proline.[40] Therefore we included the PPPP unit in all the other zwitterionic peptide sequences in this study.

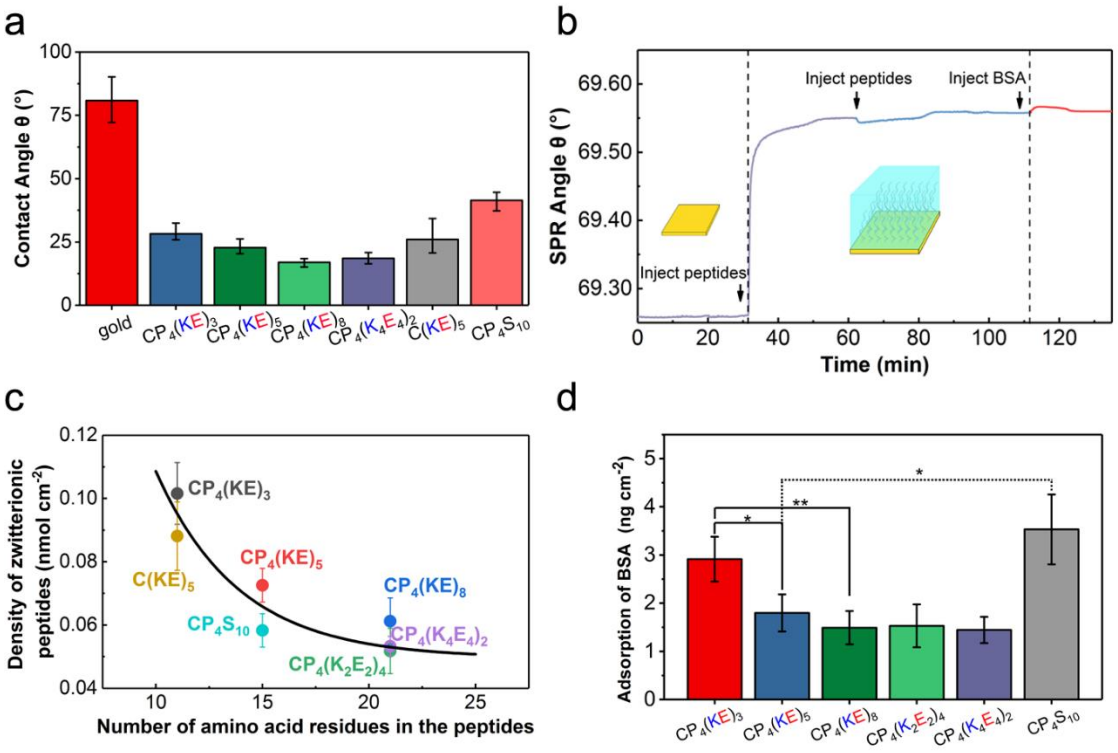

Figure 1. Antifouling behaviors of the zwitterionic peptide monolayers. (a) The static contact angle of gold surfaces modified with different zwitterionic peptide monolayers. (b) A typical SPR curve of the surface modification process following by the antifouling test. (c) The grafting density of the zwitterionic peptides decreases as a function of the peptide chain length. The fitting curve is just used for guiding the viewer's eyes. (d) The antifouling performance of the peptides with different lengths and charge distributions. (**) $p<0.01$, (*) $p<0.05$. .

We systematically tested the antifouling properties of the zwitterionic peptides using the SPR technique. Bovine album serum (BSA) and lysozyme were used as model foulants. The zwitterionic nature of the peptides is critical to their antifouling performance. When replacing the zwitterionic unit of peptide $CP_4(KE)_5$ with hydrophilic poly-serine (S_{10}) with the same

number of amino acid residues (CP_4S_{10}), the adsorption of BSA on the peptide monolayer significantly increased (Figure 1d). The charged lysine and glutamic acid residues have stronger capability of forming a hydration layer than the neutral serine residue, which is critical to the antifouling properties of the peptides. The antifouling performance of the zwitterionic peptides improves as a function of the KE repeating unit. While all the zwitterionic peptides show very low BSA adsorption (<3 ng/cm^2), increasing the KE repeating unit from 3 to 5 to 8 decreased the BSA adsorption by almost 50%, from 2.9 ng/cm^2 to 1.5 ng/cm^2. A similar but less significant trend was also observed for lysozyme (Figure S3).

The charge distribution of a zwitterionic peptide can significantly alter the structure of the peptide. It is still not clear whether a peptide with equal number of positive and negative charges but with short patchy charge distributions will have the same antifouling properties as a regular zwitterionic peptide. To study the effect of charge distributions, we systematically tested the antifouling performance of three peptides, $CP_4(KE)_8$, $CP_4(K_2E_2)_4$ and $CP_4(K_4E_4)_2$, with the same number of AA residues and zero net charge but different charge distributions. In the sequence of $CP_4(KE)_8$, the positive and negative charges are alternatively mixed whereas the sequences $CP_4(K_2E_2)_4$ and $CP_4(K_4E_4)_2$ contain a block of multiple positive charges followed by a block of negative charges, with each block carrying the same number of charges (2 or 4). As expected, three zwitterionic peptides showed very similar surface grafting density (~ 0.06 nmol/cm^2). Surprisingly, the charge distribution difference of the three peptides did not cause any difference in the antifouling properties of the peptides in PBS solution as SPR measurements showed almost identical BSA and lysozyme adsorption on the peptide monolayers (Figure 1d and Figure S3). This is likely due to the similar capabilities of the three

peptides in forming H-bond and hydration shells with the surrounding water molecules. We would come back to this in later MD simulation session.

Effect divalent cations

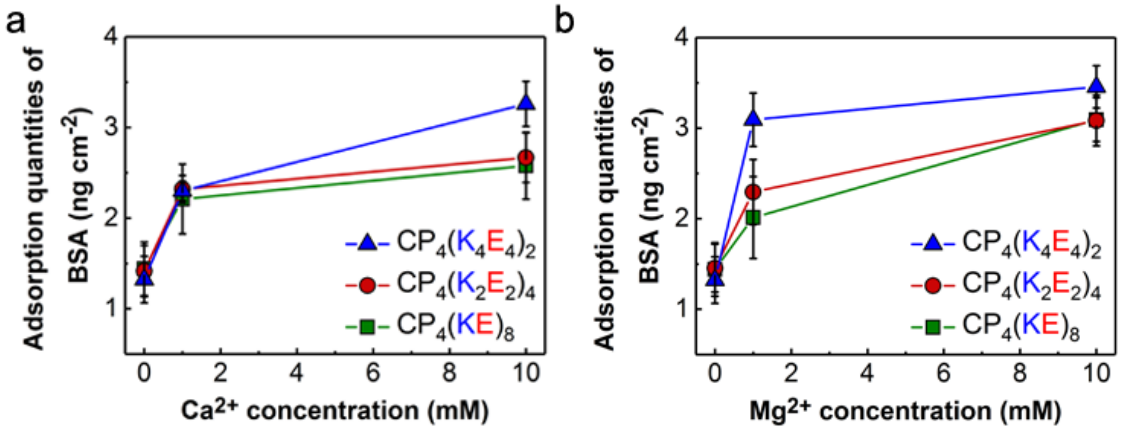

Figure 2. The effect of (a) Ca^{2+} and (b) Mg^{2+} in solution on the antifouling properties of the zwitterionic peptides.

The solution ionic environment can significantly affect the structure of zwitterionic peptide monolayers. Divalent cations, such as Ca^{2+} and Mg^{2+} widely exists in biological and natural environment, yet their effects to the antifouling properties of zwitterionic materials are not well explored. To study such effects, we compared the antifouling performance of peptides $CP_4(KE)_8$, $CP_4(K_2E_2)_4$, and $CP_4(K_4E_4)_2$ in BSA solutions with and without Ca^{2+} and Mg^{2+}. Increasing of the concentration of Ca^{2+} and Mg^{2+} in solution leads to more BSA adsorption on the peptide-modified surface for all the three zwitterionic peptides (Figure 2). The effect of the divalent cations is more pronounced for the peptide $CP_4(K_4E_4)_2$. This is likely due to the more concentrated negative charge of the sequence. Divalent cations can bridge two negative charges, which can lead to the adsorption of negatively charged BSA to the zwitterionic peptides.

Additionally, this electrostatic bridging may also lead to the structural change of the zwitterionic peptide monolayers.

The morphology and surface forces of the zwitterionic peptide monolayers.

To further understand the effect to the divalent cations, we investigate the morphology and surface forces of the zwitterionic peptide monolayers in the presence of Ca^{2+} and Mg^{2+} using an AFM. Taping model AFM images showed that the surface tethered zwitterionic peptide monolayers were homogeneous in HBS buffer (Figure 3a and Figure S4). After modifying the gold surface with a $CP_4(KE)_8$ monolayer, the average adhesion between the AFM tip and the surface decreased from 954.7 pN to 76.5 pN. Similar trend held for all the zwitterionic peptide sequences used in this study (Figure S4). In contrast, the average adhesion force between the AFM tip and a CP_4S_{10} monolayer was 626.1 pN, an order of magnitude higher than these of the zwitterionic monolayers. The low adhesion forces between the AFM tip and the peptide monolayers indicates that the zwitterionic peptide monolayers are overall neutral and well hydrated, which provide the excellent antifouling properties to the peptide monolayers.

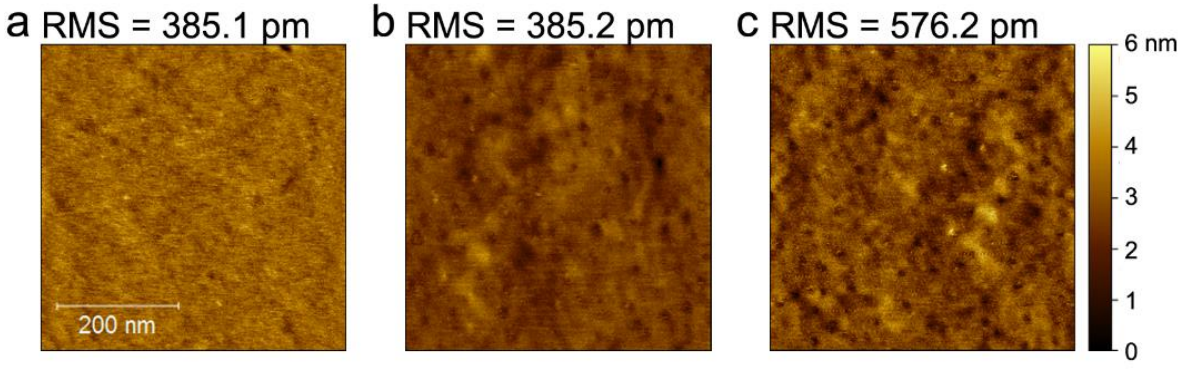

Figure 3. The morphology of the surface modified by $CP_4(KE)_8$ in (a) HBS, (b) HBS with 10 mM Ca^{2+}, and (c) HBS with 10 mM Mg^{2+}.

Adding Ca^{2+} and Mg^{2+} into the solution did not significantly alter the morphology of the zwitterionic monolayers (Figure 3) but dramatically increased the adhesion between the silicon nitride AFM tip and the zwitterionic monolayers (Figure 4c-d and Figure S5). The increase of the adhesion force is likely due to the electrostatic bridging between the peptide chains and the negatively charged AFM tip medicated by the divalent cations. The AFM adhesion measurements agreed very well with the SPR measurements, which showed an increased BSA adsorption on the zwitterionic peptide monolayers in the presence of divalent cations. As the BSA molecules are also negatively charged, Ca^{2+} and Mg^{2+} can cause adhesion between the BSA molecules and the peptide monolayers through electrostatic interactions.

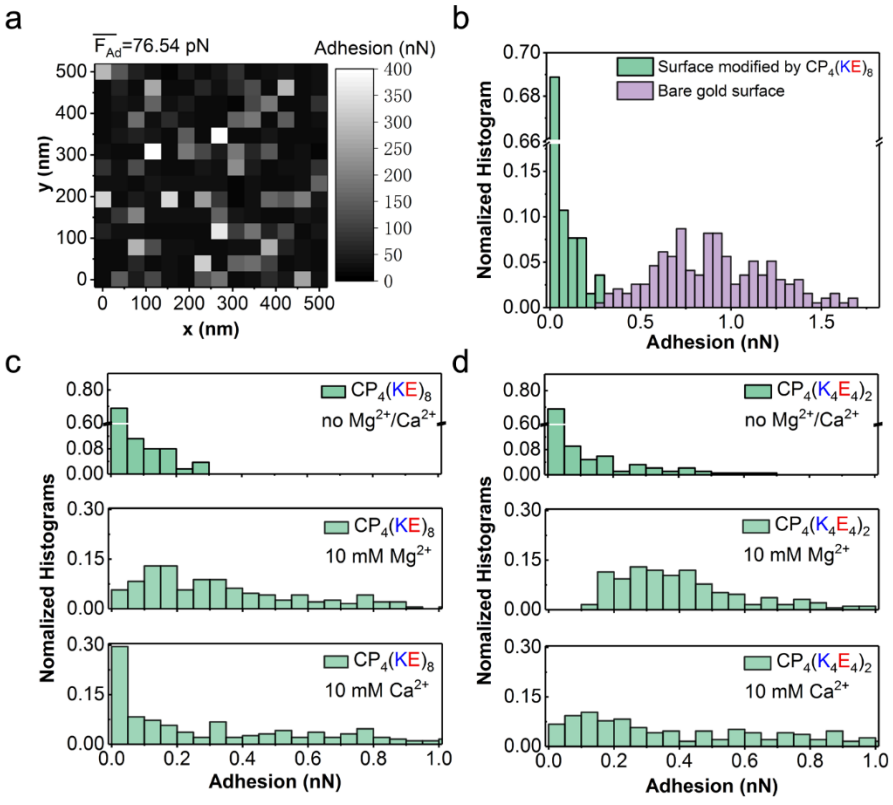

Figure 4. The adhesion distribution of the different surface in different solutions. (a) The adhesion map of the surface modified by $CP_4(KE)_8$ without divalent ions. (b) The change of the adhesion histogram after modified by $CP_4(KE)_8$. The effect of divalent ions on the adhesion

histogram of the surface modified by (c) $CP_4(KE)_8$ and (d) $CP_4(K_4E_4)_2$.

Molecular dynamics simulations of the peptides monolayers

We performed all atomistic molecular dynamics (MD) simulation to further study the molecular origin of the antifouling properties of the zwitterionic peptide monolayers. Three peptides, $CP_4(KE)_3$, $CP_4(KE)_8$ and $CP_4(K_4E_4)_2$ were simulated using GROMACS 5.1.4.[56] The grafting density of the peptides were chosen according to the SPR measurements. Firstly, we investigated the morphology of the peptide monolayers. Figure 5a shows the snapshot of a gold surface modified by $CP_4(KE)_8$ and $CP_4(K_4E_4)_2$. Due to the alternating distribution of positive and negative charges, peptide $CP_4(KE)_8$ largely exhibited inter-chain interactions as the KE repeating unit can electrostatically interact with the EK unit from another peptide chain. Salt bridges are bonds between oppositely charged residues that are sufficiently close to each.[57] The average inter-chain salt bridge per peptide chain formed by the lysine and glutamic acid residues within the same $CP_4(KE)_8$ chain (2.6 /chain) is more than the average intra-chain salt bridge per peptide (1.3 /chain) in which the lysine and glutamic acid residues are from two different peptide chains (Figure 5b). In comparison, the block charge distribution of peptide $CP_4(K_4E_4)_2$ promoted intra-chain electrostatic interactions, leading to more intra-chain salt bridges per peptide (1.9 /chain). Additionally, peptide $CP_4(K_4E_4)_2$ can form loop structures within the same chain (Figure 5a), which was not observed for $CP_4(KE)_8$.

Strong hydration is a key factor in antifouling. The number of hydrogen bond formed by a peptide chain with its surrounding water molecules is critical to its antifouling properties. MD simulation also demonstrated that longer peptides can form more hydrogen bond with

surrounding water molecules. The average hydrogen bond number formed by peptides $CP_4(KE)_8$ and $CP_4(K_4E_4)_2$ are identical, about 92 per chain, and are much larger than that of peptide $CP_4(KE)_3$. (Figure 5c). These results are consistent with the SPR measurements. The BSA adsorption on $CP_4(KE)_8$ and $CP_4(K_4E_4)_2$ modified gold surfaces were almost identical and were much smaller than that of a $CP_4(KE)_3$ monolayer. Our MD simulation results demonstrate that in monovalent salt solution, hydrophilicity is the major factor that affects the antifouling properties of the zwitterionic peptide monolayers, whereas the effect of patchy charge is not obvious.

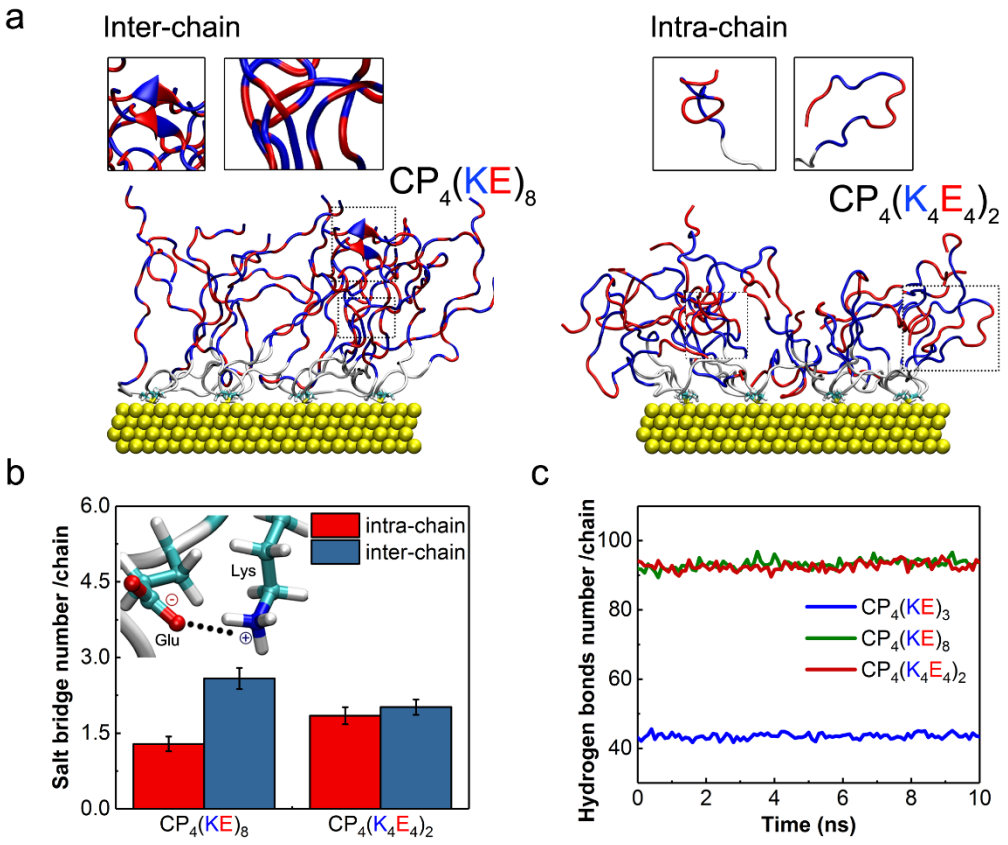

Figure 5. The molecular dynamics simulation of the peptide monolayers. (a) The snapshot of $CP_4(KE)_8$ and $CP_4(K_4E_4)_2$ monolayers on gold substrate. (b) The intra-chain/inter-chain salt bridge of $CP_4(KE)_8$ and $CP_4(K_4E_4)_2$ in which the insert shows the salt bridge between the

glutamic acid and lysine. (c) The hydrogen bonds of $CP_4(KE)_3$, $CP_4(KE)_8$ and $CP_4(K_4E_4)_2$. For the side chain in the insert of (b), red atoms are oxygen, blue atom are nitrogen, white atoms are hydrogen, and cyan atoms are carbon.

Divalent cations strongly alter the structure and hydration of the zwitterionic peptide monolayers. One divalent cations can electrostatically bridge two glutamic acid residues from the same peptide chain or different peptide chains, causing intra-chain or inter-chain electrostatic bridging (Figure 6a). Our simulation results showed that the number of inter-chain salt bridge increased as a function of divalent cation concentration (Figure 6b). Such electrostatic bridging is known to cause large structural changes to polyelectrolyte brushes.[53, 55] Additionally, the electrostatic bridging can break the overall charge neutrality of the zwitterionic peptides, leading to an overall positive charge of the peptide monolayer and more BSA adsorption. The simulation results also revealed that the average number of hydrogen bond decreased as a function of divalent cation concentration. When we increased the concentration of the divalent cations from 0 to 100 mM, the average number of hydrogen bond per chain for both $CP_4(KE)_8$ and $CP_4(K_4E_4)_2$ decreased from 93.2 per chain to 85.3 per chain. As the negatively charged glutamic acid groups are neutralized by the divalent cations, they are less capable of forming hydrogen bond with the surrounding water molecules. Therefore the zwitterionic peptides can significantly dehydrate in the presence of divalent cations, such as Ca^{2+} and Mg^{2+}, and therefore lead to a diminished antifouling performance.

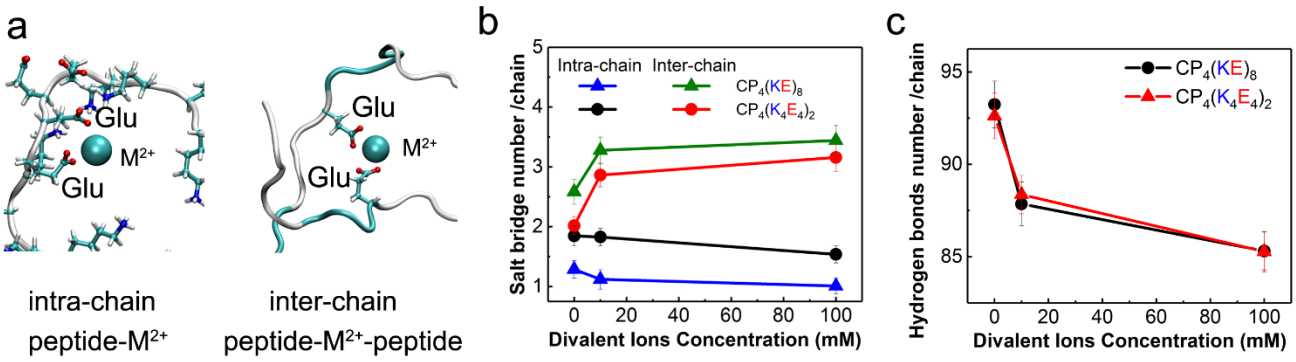

Figure 6. The molecular dynamics simulation of the peptide with divalent ions. a) The snapshot of the intra-chain salt bridge and inter-chain salt bridge. b) The salt bridge of $CP_4(KE)_8$ and $CP_4(K_4E_4)_2$ in different salt concentrations. c) The hydrogen bond of $CP_4(KE)_8$ and $CP_4(K_4E_4)_2$ in different salt concentrations.

CONCLUSION

In summary, we investigated the effect of charge distribution of the zwitterionic peptides and the existence of divalent Ca^{2+} and Mg^{2+} to the antifouling performance of natural-inspired zwitterionic peptide monolayers. By taking the advantage of controlled peptide sequences, we systematically investigated how patchy charge distribution can affect the structural and properties of zwitterionic peptides. The charge distribution can strongly alter the conformation of the zwitterionic peptides in solution. MD simulations reveal that peptides with longer block if alternating positive and negative charges show stronger intra-chain electrostatic interactions. The presence of divalent ions in solution can significantly change the surface forces of the zwitterionic peptide monolayer measured by the AFM and diminishes the antifouling performance of the zwitterionic peptides, especially the peptide sequences with patchy charge distributions. This is due to the columbic attraction between the divalent ions and glutamic acid residues, which causes dehydration of the zwitterionic peptides and electrostatic bridging

between the glutamic acid residues. Our results quantitatively demonstrated the effect of divalent cations to the structure and properties of zwitterionic peptides, which has not be carefully characterized before. The solution environment is of great importance to the properties of zwitterionic peptides. We believe that there is still a great deal to be learned on this subject. Our findings can provide critical guidance for the design novel antifouling zwitterionic peptidyl coating materials for not only anti-biofouling surfaces, but to a great realm of applications, such as medical equipment [58], drug delivery[59],medical implant[60], biosensors[61], and hygienic storage[62].

EXPERIMENTAL SECTION

Materials. All the zwitterionic peptides were obtained from Genscript (Shanghai, China) with a purity of >95%. Bovine serum albumin (BSA), lysozyme, and Tris(2-carboxyethyl)phosphine (TCEP) were purchased from Sigma-Aldrich (Beijing, China). The water used in all experiments was prepared by a three stage Millipore Milli-Q Plus 185 purification system (Millipore Corp., Bedford, MA) and had a resistivity of 18 MΩ cm. The pH values of all solutions were measured with a MP220 pH meter (Mettler Toledo, Switzerland). All solutions were filtered by 0.22 μm syringe filter before use.

Preparation of Zwitterionic Peptide monolayers. Gold-coated chips (BioNavis Ltd., Finland) were cleaned by ultrasonic cleaner (KQ-250E, KunShan Ultrasonic Instruments Co., LTD, China). The chips were then immersed in alkali piranha solution (H_2O:NH_3:H_2O_2=5:1:1) at 75 ℃ for 10 mins followed by extensive rinsing with ultrapure water and N_2 blow dry. The gold chips were placed in an ultraviolet (UV)/ozone cleaning device (PSD-UV4-Novascan,

USA) for 1 h. These chips were then rinsed with anhydrous ethanol and MilliQ water, and subsequently dried with high-purity nitrogen before use. In a typical experiment, 1 mg zwitterionic peptide was dissolved in PBS buffer (50 mM, pH 7.4) or HBS buffer (10 mM, pH 7.0) to a final concentration of 1 mg/mL. 4 mg/ml of TCEP in PBS solution was added it into peptide solutions with a ratio of 1:1 to break the disulfide bond. The final peptide concentration was adjusted to 0.015 mM.

Measurements of Modification and Nonspecific Protein Adsorption by SPR. To evaluate the performance of the Au-peptide surfaces in resisting protein adsorption, we used two single-protein solutions as test samples. BSA and lysozyme were individually dissolved in PBS to final concentrations of 1 mg/mL. A SPR Navi 200A instrument (BioNavis Ltd., Finland) equipped with a 670 nm laser as the light source was used to measure the real-time modification of the zwitterionic peptides and the nonspecific adsorption of BSA or lysozyme on the peptide modified gold chips. For each experiment, the baseline signal was established by flowing PBS buffer solution over the chip surface at a flow rate of 50 μL/min for approximately 10-20 min. The peptide solution was injected into the flow cell at a flow rate of 5 μL/min for 20 min, followed by a rinse with PBS buffer solution at 50 μL/min for 10 min. The above mentioned peptide injection was repeated one more time to ensure the gold chip was fully modified by the zwitterionic peptide. After surface modification, BSA or lysozyme solution was injected into the flow cell at a flow rate of 10 μL/min for 10 min, followed by a rinse with PBS buffer solution at 50 μL/min for 10 min. The shift in the SPR angle was recorded as the $\Delta\theta$ value, which was used to quantify the amount of peptide or protein adsorbed. When the thickness of the coating d is much smaller than the evanescent field decay length δ, the surface coverage, Γ

(here mass per area), is proportional to the resonant shift, $\Delta\theta$[63]:

$$\Gamma = \frac{\Delta\theta\delta}{2S_0 b}$$

Here δ is 218 nm by estimated from the field distribution of the surface plasmon, S_0 is the bulk sensitivity (angular shift per refractive index increment), which is 100 deg/RIU in the case of the Navi 200 A system, b is the increase in refractive index with concentration (0.184 cm^3/g is the accepted average value for proteins). A shift in the SPR angle of 1° corresponds to a surface protein adsorption of 592.4 ng/cm^2.[63]

Morphology and force curve measured by AFM. The morphology and force measurements were conducted using an Asylum Research Cypher S AFM operating in tapping mode and contact mode separately with a silicon nitride AFM probe (SiNi, BudgetSensors, force constant: 44.79 pN/nm, Amp InvOLS: 44.78 nm/V, radius is smaller than 15 nm). Experiments were performed at room temperature. Prior to measurement, the samples were rinsed with deionized water and flash-dried with nitrogen and immediately introduced to the AFM liquid cell.

Static contact angle. The static contact angles were measured using an OCA15EC device (DataPhysics Instruments, Germany), equipped with SCA 202 software. All contact angles were measured with a 5 μL water droplet deposited on test surfaces at ambient temperature. The contact angle was calculated by curve fitting the profile of the droplet from the 3-phase interface of the image captured by a CCD camera. The value for each peptide was averaged from 3 different samples with 3 separate measurements on each sample (9 measurements in total) to ensure the repeatability of the measurements.

Molecular dynamics simulations. All atomistic MD simulation was performed with

GROMACS 5.1.4.[56] Amber_99SB-ILDN force field[64] was used in conjunction with the TIP3P water model. Each simulation contains 20 peptide chains on Au (111) surface in one box, and the volume of the cubic box used in the simulations was 7.1970 × 4.9859 × 10.000 nm^3, 8.6360 ×5.9840 × 16.8360 nm^3 and 10.0750 × 5.9840 × 16.8360 nm^3 for $CP_4(KE)_3$, $CP_4(KE)_8$ and $CP_4(K_4E_4)_2$, respectively, to resemble the grafting density of each peptide in the SPR experiments. All the gold atoms and sulfur atoms were fixed during the simulation. 0.137 M NaCl were used to neutralize charges and consistent with experimental conditions. Periodic boundary conditions were used in the x- and y- directions. The system was confined between repulsive LJ walls in the z- direction with a length of 2 times of the peptide chain length. The van der Waals interactions were evaluated with a cut off of 12 Å, with energy and pressure corrections. Electrostatic interactions were evaluated using a particle-mesh Ewald sum (PME)[65], with a real space cut off of 12 Å. Correction of dispersion was used for both the energy and pressure. All these systems were first minimized by steepest-decent minimization. After energy minimization, the system was heated to the target temperature of 298.15 K for a period of 100 ps under canonical ensemble (NVT) with a time step of 2 fs. The system was equilibrated for 80 ns with a time step of 2 fs. 10 mM or 100 mM calcium chloride was then added into the system and the process mentioned above was repeated The RMSD (Root Mean Squared Deviation) become stable after 60 ns (Figure S9) and only the last 10 ns of each simulation was used for analysis. The MD simulation results were analyzed using the analysis program in the GROMACS 5.1.4 package and visual molecular dynamics (VMD).[66]

Statistical analysis. Statistical analysis was performed using student's t-test.[67] $p < 0.05$ was noted with an asterisk (*), $p < 0.01$ with two asterisks (**).

ASSOCIATED CONTENT

Supporting Information

Supplementary Figures S1−S10 and Table S1−S4: Additional SPR data, AFM morphology, AFM force map of peptides in different conditions and MD simulation results, S T-test p-value of antifouling performance, and CROMACS mdp code of molecular dynamics simulations.

AUTHOR INFORMATION

Corresponding Author

* E-mail: lisz@ntu.edu.sg

*E-mail: surx@tju.edu.cn

*E-mail: yujing@ntu.edu.sg

Author Contributions

Chuanxi Li and Chunjiang Liu contributed equally to this work.

Notes

The authors declare no competing financial interest.

ACKNOWLEDGEMENTS

CX L, CJ L, and RX S acknowledge the National Natural Science Foundation of China (21621004), Tianjin Municipal Science and Technology Bureau, China (16JCZDJC37900), the

Ministry of Education (grant No. NCET-11-0372), and the financial support from China Scholarship Council (CSC, 201806250100). M L and J Y thanks to Singapore Ministry of Education Academic Research Fund Tier 1 (RG7/19) and the Singapore National Research Fellowship (NRF-NRFF11-2019-0004). We would like to thank Dr. Daniel Daniel for his help in our AFM experiment.

REFERENCES

(1) Ratner, B. D.; Bryant, S. J. Biomaterials: Where we have been and where we are going. *Annu Rev Biomed Eng* **2004,** *6*, 41-75.
(2) Lee, H.; Dellatore, S. M.; Miller, W. M.; Messersmith, P. B. Mussel-inspired surface chemistry for multifunctional coatings. *Science* **2007,** *318* (5849), 426-30.
(3) Langer, R. Drug delivery. Drugs on target. *Science* **2001,** *293* (5527), 58-9.
(4) Wu, J.; Han, H.; Jin, Q.; Li, Z.; Li, H.; Ji, J. Design and proof of programmed 5-aminolevulinic acid prodrug nanocarriers for targeted photodynamic cancer therapy. *ACS Appl. Mater. Interfaces* **2017,** *9* (17), 14596-14605.
(5) Wei, Q.; Becherer, T.; Angioletti-Uberti, S.; Dzubiella, J.; Wischke, C.; Neffe, A. T.; Lendlein, A.; Ballauff, M.; Haag, R. Protein interactions with polymer coatings and biomaterials. *Angew. Chem. Int. Ed. Engl.* **2014,** *53* (31), 8004-31.
(6) Li, Y. X.; Wang, L.; Ding, C. F.; Luo, X. L. Highly selective ratiometric electrogenerated chemiluminescence assay of DNA methyltransferase activity via polyaniline and anti-fouling peptide modified electrode. *Biosens. Bioelectron.* **2019,** *142*, 111553.
(7) Krishnamoorthy, M.; Hakobyan, S.; Ramstedt, M.; Gautrot, J. E. Surface-initiated polymer brushes in the biomedical field: applications in membrane science, biosensing, cell culture, regenerative medicine and antibacterial coatings. *Chem. Rev.* **2014,** *114* (21), 10976-1026.
(8) Banerjee, I.; Pangule, R. C.; Kane, R. S. Antifouling coatings: recent developments in the design of surfaces that prevent fouling by proteins, bacteria, and marine organisms. *Adv. Mater.* **2011,** *23* (6), 690-718.
(9) Bixler, G. D.; Bhushan, B. Biofouling: lessons from nature. *Philos Trans A Math Phys Eng Sci* **2012,** *370* (1967), 2381-417.
(10) Chen, Q.; Yu, S.; Zhang, D. H.; Zhang, W. J.; Zhang, H. D.; Zou, J. C.; Mao, Z. W.; Yuan, Y.; Gao, C. Y.; Liu, R. H. Impact of Antifouling PEG Layer on the Performance of Functional Peptides in Regulating Cell Behaviors. *J. Am. Chem. Soc.* **2019,** *141* (42), 16772-16780.
(11) Qian, H. S.; Huang, Y.; Duan, X. L.; Wei, X. T.; Fan, Y. P.; Gan, D. L.; Yue, S. J.; Cheng, W.; Chen, T. M. Fiber optic surface plasmon resonance biosensor for detection of PDGF-BB in serum based on self-assembled aptamer and antifouling peptide monolayer. *Biosens. Bioelectron.* **2019,** *140*, 90-95.
(12) Herrwerth, S.; Eck, W.; Reinhardt, S.; Grunze, M. Factors that determine the protein

resistance of oligoether self-assembled monolayers - Internal hydrophilicity, terminal hydrophilicity, and lateral packing density. *J. Am. Chem. Soc.* **2003,** *125* (31), 9359-9366.
(13) Unsworth, L. D.; Sheardown, H.; Brash, J. L. Protein resistance of surfaces prepared by sorption of end-thiolated poly(ethylene glycol) to gold: effect of surface chain density. *Langmuir* **2005,** *21* (3), 1036-41.
(14) Sileika, T. S.; Kim, H. D.; Maniak, P.; Messersmith, P. B. Antibacterial performance of polydopamine-modified polymer surfaces containing passive and active components. *ACS Appl. Mater. Interfaces* **2011,** *3* (12), 4602-10.
(15) Emilsson, G.; Schoch, R. L.; Feuz, L.; Hook, F.; Lim, R. Y.; Dahlin, A. B. Strongly stretched protein resistant poly(ethylene glycol) brushes prepared by grafting-to. *ACS Appl. Mater. Interfaces* **2015,** *7* (14), 7505-15.
(16) Li, L.; Yan, B.; Yang, J.; Chen, L.; Zeng, H. Novel mussel-inspired injectable self-healing hydrogel with anti-biofouling property. *Adv. Mater.* **2015,** *27* (7), 1294-9.
(17) Kim, S.; Gim, T.; Kang, S. M. Versatile, tannic acid-mediated surface PEGylation for marine antifouling applications. *ACS Appl. Mater. Interfaces* **2015,** *7* (12), 6412-6.
(18) Xu, X.; Billing, M.; Ruths, M.; Klok, H. A.; Yu, J. Structure and Functionality of Polyelectrolyte Brushes: A Surface Force Perspective. *Chem-Asian J* **2018,** *13* (22), 3411-3436.
(19) Greene, G. W.; Martin, L. L.; Tabor, R. F.; Michalczyk, A.; Ackland, L. M.; Horn, R. Lubricin: a versatile, biological anti-adhesive with properties comparable to polyethylene glycol. *Biomaterials* **2015,** *53*, 127-36.
(20) Webster, R.; Didier, E.; Harris, P.; Siegel, N.; Stadler, J.; Tilbury, L.; Smith, D. A. PEGylated proteins: evaluation of their safety in the absence of definitive metabolism studies. *Drug Metab. Disposition* **2006**.
(21) Arima, Y.; Toda, M.; Iwata, H. Complement activation on surfaces modified with ethylene glycol units. *Biomaterials* **2008,** *29* (5), 551-60.
(22) Ederth, T.; Lerm, M.; Orihuela, B.; Rittschof, D. Resistance of Zwitterionic Peptide Monolayers to Biofouling. *Langmuir* **2019,** *35* (5), 1818-1827.
(23) Jiang, S. Y.; Cao, Z. Q. Ultralow-Fouling, Functionalizable, and Hydrolyzable Zwitterionic Materials and Their Derivatives for Biological Applications. *Adv. Mater.* **2010,** *22* (9), 920-932.
(24) Blaszykowski, C.; Sheikh, S.; Thompson, M. Surface chemistry to minimize fouling from blood-based fluids. *Chem. Soc. Rev.* **2012,** *41* (17), 5599-612.
(25) Lu, X.; Nicovich, P. R.; Zhao, M. C.; Nieves, D. J.; Mollazade, M.; Vivekchand, S. R. C.; Gaus, K.; Gooding, J. J. Monolayer surface chemistry enables 2-colour single molecule localisation microscopy of adhesive ligands and adhesion proteins. *Nat. Commun.* **2018,** *9* (1), 3320.
(26) Roberts, J. N.; Sahoo, J. K.; McNamara, L. E.; Burgess, K. V.; Yang, J. L.; Alakpa, E. V.; Anderson, H. J.; Hay, J.; Turner, L. A.; Yarwood, S. J.; Zelzer, M.; Oreffo, R. O. C.; Ulijn, R. V.; Dalby, M. J. Dynamic Surfaces for the Study of Mesenchymal Stem Cell Growth through Adhesion Regulation. *ACS Nano* **2016,** *10* (7), 6667-6679.
(27) Cheng, G.; Xue, H.; Zhang, Z.; Chen, S.; Jiang, S. A switchable biocompatible polymer surface with self-sterilizing and nonfouling capabilities. *Angew. Chem. Int. Ed. Engl.* **2008,** *47* (46), 8831-4.
(28) Zhang, Z.; Chen, S.; Jiang, S. Dual-functional biomimetic materials: nonfouling

poly(carboxybetaine) with active functional groups for protein immobilization. *Biomacromolecules* **2006,** *7* (12), 3311-5.
(29) Chen, S.; Zheng, J.; Li, L.; Jiang, S. Strong resistance of phosphorylcholine self-assembled monolayers to protein adsorption: insights into nonfouling properties of zwitterionic materials. *J. Am. Chem. Soc.* **2005,** *127* (41), 14473-8.
(30) Gao, C.; Li, G.; Xue, H.; Yang, W.; Zhang, F.; Jiang, S. Functionalizable and ultra-low fouling zwitterionic surfaces via adhesive mussel mimetic linkages. *Biomaterials* **2010,** *31* (7), 1486-92.
(31) Cao, Z. Q.; Jiang, S. Y. Super-hydrophilic zwitterionic poly(carboxybetaine) and amphiphilic non-ionic poly(ethylene glycol) for stealth nanoparticles. *Nano Today* **2012,** *7* (5), 404-413.
(32) Huang, C. J.; Li, Y.; Jiang, S. Zwitterionic polymer-based platform with two-layer architecture for ultra low fouling and high protein loading. *Anal. Chem.* **2012,** *84* (7), 3440-5.
(33) Mi, L.; Jiang, S. Integrated antimicrobial and nonfouling zwitterionic polymers. *Angew. Chem. Int. Ed. Engl.* **2014,** *53* (7), 1746-54.
(34) Shao, Q.; Jiang, S. Molecular understanding and design of zwitterionic materials. *Adv. Mater.* **2015,** *27* (1), 15-26.
(35) Yang, W.; Xue, H.; Carr, L. R.; Wang, J.; Jiang, S. Zwitterionic poly(carboxybetaine) hydrogels for glucose biosensors in complex media. *Biosens. Bioelectron.* **2011,** *26* (5), 2454-9.
(36) Zhao, C.; Zhao, J.; Li, X.; Wu, J.; Chen, S.; Chen, Q.; Wang, Q.; Gong, X.; Li, L.; Zheng, J. Probing structure-antifouling activity relationships of polyacrylamides and polyacrylates. *Biomaterials* **2013,** *34* (20), 4714-24.
(37) Wang, G.; Han, R.; Su, X.; Li, Y.; Xu, G.; Luo, X. Zwitterionic peptide anchored to conducting polymer PEDOT for the development of antifouling and ultrasensitive electrochemical DNA sensor. *Biosens. Bioelectron.* **2017,** *92*, 396-401.
(38) Aili, D.; Stevens, M. M. Bioresponsive peptide-inorganic hybrid nanomaterials. *Chem. Soc. Rev.* **2010,** *39* (9), 3358-70.
(39) Ramakers, B. E.; van Hest, J. C.; Lowik, D. W. Molecular tools for the construction of peptide-based materials. *Chem. Soc. Rev.* **2014,** *43* (8), 2743-56.
(40) Nowinski, A. K.; Sun, F.; White, A. D.; Keefe, A. J.; Jiang, S. Sequence, structure, and function of peptide self-assembled monolayers. *J. Am. Chem. Soc.* **2012,** *134* (13), 6000-5.
(41) Khatayevich, D.; Gungormus, M.; Yazici, H.; So, C.; Cetinel, S.; Ma, H.; Jen, A.; Tamerler, C.; Sarikaya, M. Biofunctionalization of materials for implants using engineered peptides. *Acta Biomater.* **2010,** *6* (12), 4634-41.
(42) Bolduc, O. R.; Pelletier, J. N.; Masson, J. F. SPR Biosensing in crude serum using ultralow fouling binary patterned peptide SAM. *Anal. Chem.* **2010,** *82* (9), 3699-706.
(43) Alvarez-Martos, I.; Moller, A.; Ferapontova, E. E. Dopamine Binding and Analysis in Undiluted Human Serum and Blood by the RNA-Aptamer Electrode. *ACS Chem. Neurosci.* **2019,** *10* (3), 1706-1715.
(44) Wu, L. M.; Lin, B. Y.; Yang, H.; Chen, J.; Mao, Z. W.; Wang, W. L.; Gao, C. Y. Enzyme-responsive multifunctional peptide coating of gold nanorods improves tumor targeting and photothermal therapy efficacy. *Acta Biomaterialia* **2019,** *86*, 363-372.
(45) Wang, L.; Shi, C.; Wang, X.; Guo, D.; Duncan, T. M.; Luo, J. Zwitterionic Janus

Dendrimer with distinct functional disparity for enhanced protein delivery. *Biomaterials* **2019,** *215*, 119233.
(46) Yang, Q. H.; Wang, L. G.; Lin, W. F.; Ma, G. L.; Yuan, J.; Chen, S. F. Development of nonfouling polypeptides with uniform alternating charges by polycondensation of the covalently bonded dimer of glutamic acid and lysine. *J. Mater. Chem. B* **2014,** *2* (5), 577-584.
(47) Qi, H. S.; Zheng, W. W.; Zhang, C.; Zhou, X.; Zhang, L. Novel Mussel-Inspired Universal Surface Functionalization Strategy: Protein-Based Coating with Residue-Specific Post-Translational Modification in Vivo. *ACS Appl. Mater. Interfaces* **2019,** *11* (13), 12846-12853.
(48) Feng, Y.; Wang, Q.; He, M.; Zhang, X.; Liu, X.; Zhao, C. Antibiofouling Zwitterionic Gradational Membranes with Moisture Retention Capability and Sustained Antimicrobial Property for Chronic Wound Infection and Skin Regeneration. *Biomacromolecules* **2019,** *20* (8), 3057-3069.
(49) Chen, S.; Cao, Z.; Jiang, S. Ultra-low fouling peptide surfaces derived from natural amino acids. *Biomaterials* **2009,** *30* (29), 5892-6.
(50) Keefe, A. J.; Caldwell, K. B.; Nowinski, A. K.; White, A. D.; Thakkar, A.; Jiang, S. Screening nonspecific interactions of peptides without background interference. *Biomaterials* **2013,** *34* (8), 1871-7.
(51) Ziemba, C.; Khavkin, M.; Priftis, D.; Acar, H.; Mao, J.; Benami, M.; Gottlieb, M.; Tirrell, M.; Kaufman, Y.; Herzberg, M. Antifouling Properties of a Self-Assembling Glutamic Acid-Lysine Zwitterionic Polymer Surface Coating. *Langmuir* **2019,** *35* (5), 1699-1713.
(52) Zhang, H. T.; Sun, A. Y.; Kim, J. J.; Graham, V.; Finch, E. A.; Nepliouev, I.; Zhao, G. L.; Li, T. Y.; Lederer, W. J.; Stiber, J. A.; Pitt, G. S.; Bursac, N.; Rosenberg, P. B. STIM1-Ca2+ signaling modulates automaticity of the mouse sinoatrial node. *PNAS* **2015,** *112* (41), E5618-E5627.
(53) Yu, J.; Jackson, N. E.; Xu, X.; Morgenstern, Y.; Kaufman, Y.; Ruths, M.; de Pablo, J. J.; Tirrell, M. Multivalent counterions diminish the lubricity of polyelectrolyte brushes. *Science* **2018,** *360* (6396), 1434-1438.
(54) Yu, J.; Jackson, N. E.; Xu, X.; Brettmann, B. K.; Ruths, M.; de Pablo, J. J.; Tirrell, M. Multivalent ions induce lateral structural inhomogeneities in polyelectrolyte brushes. *Sci. Adv.* **2017,** *3* (12), eaao1497.
(55) Xu, X.; Mastropietro, D.; Ruths, M.; Tirrell, M.; Yu, J. Ion-Specific Effects of Divalent Ions on the Structure of Polyelectrolyte Brushes. *Langmuir* **2019**.
(56) Pronk, S.; Pall, S.; Schulz, R.; Larsson, P.; Bjelkmar, P.; Apostolov, R.; Shirts, M. R.; Smith, J. C.; Kasson, P. M.; van der Spoel, D.; Hess, B.; Lindahl, E. GROMACS 4.5: a high-throughput and highly parallel open source molecular simulation toolkit. *Bioinformatics* **2013,** *29* (7), 845-54.
(57) Bosshard, H. R.; Marti, D. N.; Jelesarov, I. Protein stabilization by salt bridges: concepts, experimental approaches and clarification of some misunderstandings. *J. Mol. Recognit.* **2004,** *17* (1), 1-16.
(58) Pavithra, D.; Doble, M. Biofilm formation, bacterial adhesion and host response on polymeric implants - issues and prevention. *Biomed. Mater.* **2008,** *3* (3), 034003.
(59) Jin, Q.; Deng, Y.; Chen, X.; Ji, J. Rational Design of Cancer Nanomedicine for Simultaneous Stealth Surface and Enhanced Cellular Uptake. *ACS Nano* **2019,** *13* (2), 954-977.
(60) Chang, J.; Tao, Y.; Wang, B.; Guo, B. H.; Xu, H.; Jiang, Y. R.; Huang, Y. B. An in situ-

forming zwitterionic hydrogel as vitreous substitute. *J. Mater. Chem. B* **2015,** *3* (6), 1097-1105.
(61) Sabaté del Río, J.; Henry, O. Y. F.; Jolly, P.; Ingber, D. E. An antifouling coating that enables affinity-based electrochemical biosensing in complex biological fluids. *Nat. Nanotech.* **2019**.
(62) Kenawy, E. R.; Worley, S. D.; Broughton, R. The chemistry and applications of antimicrobial polymers: A state-of-the-art review. *Biomacromolecules* **2007,** *8* (5), 1359-1384.
(63) Ye, H. J.; Xia, Y. Q.; Liu, Z. Q.; Huang, R. L.; Su, R. X.; Qi, W.; Wang, L. B.; He, Z. M. Dopamine-assisted deposition and zwitteration of hyaluronic acid for the nanoscale fabrication of low-fouling surfaces. *J. Mater. Chem. B* **2016,** *4* (23), 4084-4091.
(64) Lindorff-Larsen, K.; Piana, S.; Palmo, K.; Maragakis, P.; Klepeis, J. L.; Dror, R. O.; Shaw, D. E. Improved side-chain torsion potentials for the Amber ff99SB protein force field. *Proteins* **2010,** *78* (8), 1950-8.
(65) Darden, T.; York, D.; Pedersen, L. Particle mesh Ewald: An N· log (N) method for Ewald sums in large systems. *J. Chem. Phys.* **1993,** *98* (12), 10089-10092.
(66) Humphrey, W.; Dalke, A.; Schulten, K. VMD: visual molecular dynamics. *J Mol Graph* **1996,** *14* (1), 33-8, 27-8.
(67) Kalpić, D.; Hlupić, N.; Lovrić, M., Student's t-Tests. In *International Encyclopedia of Statistical Science*, Lovric, M., Ed. Springer Berlin Heidelberg: Berlin, Heidelberg, 2011; pp 1559-1563.

TOC

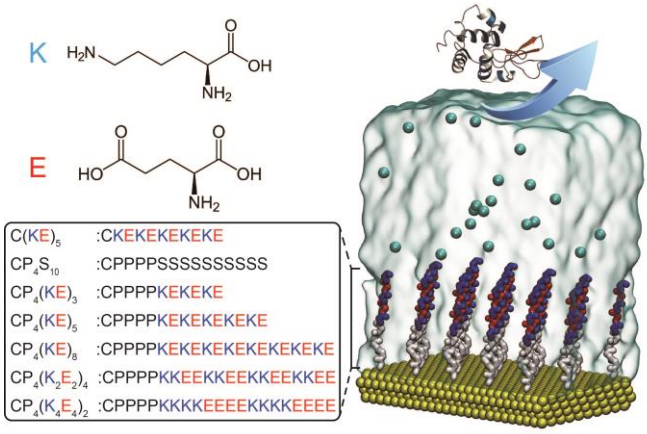
K
E
C(KE)5 :CKEKEKEKEKE
CP4S10 :CPPPPSSSSSSSSSS
CP4(KE)3 :CPPPPKEKEKE
CP4(KE)5 :CPPPPKEKEKEKEKE
CP4(KE)8 :CPPPPKEKEKEKEKEKEKEKE
CP4(K2E2)4 :CPPPPKKEEKKEEKKEEKKEE
CP4(K4E4)2 :CPPPPKKKKEEEEKKKKEEEE